ADVANCED FUNCTIONAL MATERIALS
www.afm-journal.de

Electronic Structure and Optoelectronic Properties of Bismuth Oxyiodide Robust against Percent-Level Iodine-, Oxygen-, and Bismuth-Related Surface Defects

*Tahmida N. Huq, Lana C. Lee, Lissa Eyre, Weiwei Li, Robert A. Jagt, Chaewon Kim, Sarah Fearn, Vincenzo Pecunia, Felix Deschler, Judith L. MacManus-Driscoll, and Robert L. Z. Hoye**

In the search for nontoxic alternatives to lead-halide perovskites, bismuth oxyiodide (BiOI) has emerged as a promising contender. BiOI is air-stable for over three months, demonstrates promising early-stage photovoltaic performance and, importantly, is predicted from calculations to tolerate vacancy and antisite defects. Here, whether BiOI tolerates point defects is experimentally investigated. BiOI thin films are annealed at a low temperature of 100 °C under vacuum (25 Pa absolute pressure). There is a relative reduction in the surface atomic fraction of iodine by over 40%, reduction in the surface bismuth fraction by over 5%, and an increase in the surface oxygen fraction by over 45%. Unexpectedly, the Bi $4f_{7/2}$ core level position, Fermi level position, and valence band density of states of BiOI are not significantly changed. Further, the charge-carrier lifetime, photoluminescence intensity, and the performance of the vacuum-annealed BiOI films in solar cells remain unchanged. The results show BiOI to be electronically and optoelectronically robust to percent-level changes in surface composition. However, from photoinduced current transient spectroscopy measurements, it is found that the as-grown BiOI films have deep traps located ≈0.3 and 0.6 eV from the band edge. These traps limit the charge-carrier lifetimes of BiOI, and future improvements in the performance of BiOI photovoltaics will need to focus on identifying their origin. Nevertheless, these deep traps are three to four orders of magnitude less concentrated than the surface point defects induced through vacuum annealing. The charge-carrier lifetimes of the BiOI films are also orders of magnitude longer than if these surface defects were recombination active. This work therefore shows BiOI to be robust against processing conditions that lead to percent-level iodine-, bismuth-, and oxygen-related surface defects. This will simplify and reduce the cost of fabricating BiOI-based electronic devices, and stands in contrast to the defect-sensitivity of traditional covalent semiconductors.

T. N. Huq, Dr. L. C. Lee, Dr. W.-W. Li, R. A. Jagt,
Prof. J. L. MacManus-Driscoll, Dr. R. L. Z. Hoye
Department of Materials Science and Metallurgy
University of Cambridge
27 Charles Babbage Road, Cambridge CB3 0FS, UK
E-mail: r.hoye@imperial.ac.uk

L. Eyre
Department of Physics
University of Cambridge
JJ Thomson Ave, Cambridge CB3 0HE, UK

The ORCID identification number(s) for the author(s) of this article can be found under https://doi.org/10.1002/adfm.201909983.

DOI: 10.1002/adfm.201909983

L. Eyre, Dr. F. Deschler
Walter Schottky Institute
Department of Physics
Technical University of Munich
Am Coulombwall 4, 85748 Garching, Germany

Dr. C. Kim, Dr. V. Pecunia
Institute of Functional Nano & Soft Materials (FUNSOM)
Jiangsu Key Laboratory for Carbon-Based Functional Materials & Devices
Soochow University
199 Ren'ai Road, Suzhou, 215123 Jiangsu, P. R. China

Dr. S. Fearn, Dr. R. L. Z. Hoye
Department of Materials
Imperial College London
Exhibition Road, London SW7 2AZ, UK

1. Introduction

Photovoltaics based on lead-halide perovskites (LHPs) have rapidly risen in efficiency,[1] which, surprisingly, was achieved using low-temperature solution-based fabrication methods.[2] The key enabling properties of LHPs are high absorption coefficients,[3] low Urbach energies,[4] high luminescence quantum yields,[5] low exciton binding energies,[6] and long minority-carrier lifetimes.[7,8] Critically, LHPs exhibit tolerance toward intrinsic[9,10] and a range of extrinsic defects,[11,12] which allow low nonradiative recombination rates to occur despite high defect densities.[13] Defect tolerance has enabled LHP thin films with high optoelectronic quality to be achieved by multiple groups using facile processing equipment, which has contributed to the fast cycles of learning.[14] Although LHPs do have deep traps that need to be passivated in order to achieve record power conversion efficiencies,[15,16] computational investigations have shown that most point defects form shallow transition levels.[13,17] As such, polycrystalline LHP thin films, which have typical trap densities of 10^{15}–10^{17} cm^{-3},[18–21] can still achieve technologically relevant power conversion efficiencies >15% in photovoltaic devices without intentionally passivating the bulk or surfaces.[16,22,23] Recently, it was shown that methylammonium lead iodide ($MAPbI_3$) can tolerate one pair of methylammonium and iodine vacancies per $[PbI_6]^{4-}$ octahedron before significant changes to the electronic structure occur.[24] This is consistent with predictions of self-regulation to charged point defects in LHPs.[9,24,25] The tolerance of the electronic structure of $MAPbI_3$ to percent-level changes in I content is consistent with observations that the performance of $MAPbI_3$ solar cells is not completely deteriorated when the stoichiometry of MAI to PbI_2 in the precursor solution is varied at the percent level.[26] $CuInSe_2$ has also been previously found to tolerate native defect densities at the percent level, and this was accounted for by In_{Cu} antisite defects forming a benign defect pair with V_{Cu}.[27] The defect tolerance of LHPs and $CuInSe_2$ are in stark contrast to the defect-sensitivity of traditional covalent semiconductors (e.g., silicon or GaAs), in which defect densities several orders of magnitude below the percent level are required for them to operate efficiently in electronic devices.[24,28] When fabricating electronic devices from these defect-sensitive materials, care needs to be taken to avoid inducing the formation of any point defects.

While the efficiency, stability, and understanding of LHPs are rapidly increasing, the toxicity and soluble nature of the lead component[29,30] has led to interest in lead-free alternatives.[17] At the same time, emphasis has been placed on alternatives that are also composed of abundant elements, in contrast to $CuInSe_2$, in which the scarcity of In is a limiting factor.[31] An outstanding question in the field is how the defect tolerance of the LHPs arises and whether this property can be replicated in other classes of lead-free materials. An early model developed was based on the electronic structure, in which the arrangement of the bonding–antibonding orbitals formed from the hybridization of Pb 6s, Pb 6p, and I 5p orbitals results in an increased likelihood of traps being resonant within one of the bands or shallow within the bandgap.[32] This led to the prediction that compounds based on cations with stable valence pairs of s electrons (e.g., Bi^{3+}, In^{+}, Sn^{2+}, or Sb^{3+}) may replicate the perovskite electronic structure and its defect tolerance.[33] More recent work has shown that the energy alignment between cation/anion orbitals and spacing between ions also play a significant role.[33] Nevertheless, having a partially oxidized cation with a stable valence pair of s electrons remains an important factor for achieving predominantly shallow traps.[33] These ns^2 compounds have recently gained significant interest, with many materials demonstrating promising bulk properties for photovoltaic applications and improved ambient stabilities over LHPs.[33–36] One such material is bismuth oxyiodide (BiOI). Bismuth-based compounds have the important advantages of exhibiting very little evidence of toxicity,[37] and bismuth is sufficiently abundant for commercialization in photovoltaics,[38] with the production of bismuth being two orders of magnitude larger than that of indium.[31] We previously measured the bandgap of BiOI to be 1.9 eV, and the absorption coefficient to be on the order of 10^4 cm^{-1} above the band edge.[38] While the bandgap is wider and absorption coefficient smaller than the related BiI_3 compound (1.67 eV and $\approx 10^5$ cm^{-1}, respectively),[39] the bandgap of BiOI is close to the optimum for top cells in four-terminal tandems with silicon, and the absorption coefficient adequate for achieving a spectroscopically limited maximum efficiency exceeding 20% in single-junction devices.[38] The BiOI solar cells we previously made and tested achieved a high external quantum efficiency (EQE) of 80% at 450 nm wavelength, which exceeds the EQEs that have been achieved with BiI_3 solar cells so far.[38,40,41] We also demonstrated BiOI to be phase-stable in ambient air for at least 197 d,[38,42] whereas $MAPbI_3$ thin films degraded within 5 d under similar conditions.[36] The BiOI devices remained stable in air over the 3 d that we tested them, whereas $MAPbI_3$ solar cells using a similar architecture (NiO_x hole transport layer on the bottom; Al electrode on top) degraded within minutes in air.[38] Critically, defect calculations showed that the lowest formation energy point defects in BiOI (iodine vacancies, bismuth vacancies, and oxygen-on-iodine antisites or V_I, V_{Bi}, and O_I) have transition levels that are either resonant within the bands or are shallow within the bandgap. These computations are consistent with predictions and indicate BiOI to be tolerant to the vacancy and antisite defects investigated computationally.[38] Thus, BiOI has potential for photovoltaic applications, while being significantly more stable than $MAPbI_3$.

However, experimental evidence for defect tolerance in BiOI as well as other ns^2 compounds is lacking in the field. Systematic measurements to understand the role of defects in these materials are critical to test current models for defect tolerance and quantify the extent to which these materials are able to tolerate point defects. In this work, we induce the formation of point defects by annealing under medium vacuum (25 Pa absolute pressure) at 100 °C, which corresponds to a sufficiently low homologous temperature to not result in structural changes or reduce the phase purity.[43] This was to remove iodine (to form V_I) and, to a lesser extent, bismuth (to form V_{Bi}). We use a combination of techniques to quantify the changes in composition, electronic structure, luminescence, charge-carrier lifetime, and crystal structure. To correlate these effects on the impact on device performance, we fabricate full devices from BiOI thin films vacuum annealed for up to 180 min. Our work provides valuable new experimental insight into the tolerance of the electronic and optoelectronic properties of BiOI to point defects.

More broadly, the vacuum annealing conditions used are similar to the vacuum conditions and/or heating experienced by BiOI thin films when subsequent layers are deposited on top (e.g., by vacuum-based atomic layer deposition, chemical vapor deposition, or thermal evaporation). As such, our work also determines how stringently a pristine surface in BiOI needs to be maintained in device fabrication, which affects the cost of production.

2. Results

To investigate the effect of vacuum annealing on the composition, and the associated effect on the Fermi level position, we performed X-ray photoemission spectroscopy (XPS) measurements. This allowed us to obtain both the composition and Fermi level position (from core level and valence band spectra, respectively), measured from the same interaction volume. In our system, the sample depth was between 1 and 3 nm. We grew BiOI thin films according to our previous report,[38] and found the surface composition in the as-grown films to be close to stoichiometric (shown by the dashed lines in **Figure 1**a). After vacuum annealing at 100 °C for 5 s through to 2 d, the fraction of iodine measured at the surface significantly decreased from 0.33 (no vacuum annealing) to 0.18 (10 min vacuum annealing), before decreasing more slowly to 0.15–0.16 after 1–2 d. By contrast, the surface oxygen fraction increased at a higher rate than the decrease in iodine fraction, appearing to saturate at a fraction of ≈0.6 (Figure 1b). There was initially very little change in the fraction of bismuth for up to 1 min vacuum annealing, before decreasing from a fraction of 0.37 (no annealing) to 0.3 and saturating (Figure 1a).

Despite the significant changes in composition, the binding energy of the Bi $4f_{7/2}$ core level remained between 158.65 and 158.9 eV over the entire vacuum annealing series (Figure 1c). This variation in core level binding energy is much smaller than if second phases occurred (see Discussion), and is accounted for by the changes in the bonding environment for Bi^{3+} as the surface composition changed. XPS measurements also showed that the Fermi level position relative to the valence band maximum (E_F–VB) remained unchanged over the vacuum annealing series (Figure 1d). No change in the shape of the valence band density of states was observed with vacuum annealing (Figures S1 and S2, Supporting Information), nor did we observe the valence band spectra to change during the XPS measurements when the films were exposed to ultrahigh vacuum and X-ray photons ($h\nu$ = 1486.6 eV). The XPS data show the electronic structure of BiOI to be robust to distributed defects. Indeed, these results show BiOI to be more robust than methylammonium lead iodide perovskite. Previous reports by Steirer et al. found the E_F–VB and Pb $4f_{7/2}$ core peak to shift in energy when the I/Pb ratio decreased below 2.5, as a second phase of PbI_2 began to form.[24] By contrast, no changes in the

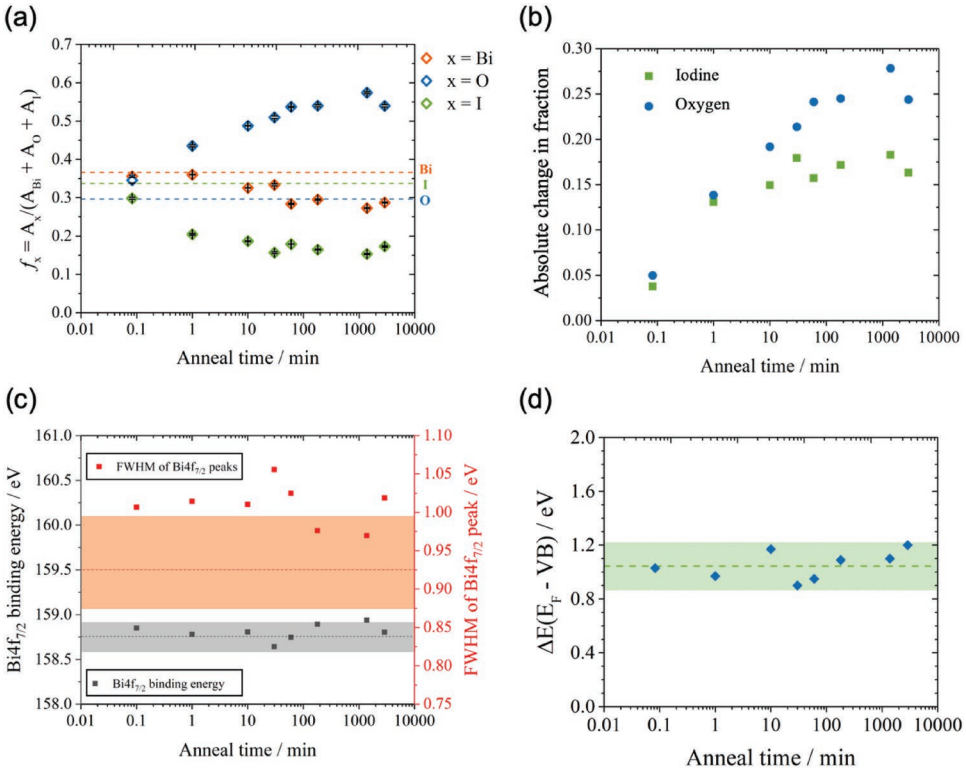

Figure 1. Effect of vacuum annealing BiOI at 100 °C and 25 Pa absolute pressure. a) Atomic fractions of Bi, O, and I (f_x where x = Bi, O, I) determined from XPS core level spectra. The dashed lines represent the average fraction of Bi (orange), O (blue), and I (green) in eight BiOI films before annealing. The error bars displayed represent the uncertainty determined by fitting the same spectrum five times. b) Absolute change in the fraction of oxygen and iodine from original values before annealing. c) Binding energy and full width at half maximum (FWHM) of Bi $4f_{7/2}$ core level peaks for BiOI samples after vacuum annealing. d) Fermi level offset from the valence band maximum of BiOI. In both (c) and (d), the colored line represents the mean value of eight samples before annealing, and the shaded box represents two standard deviations on either side of the mean.

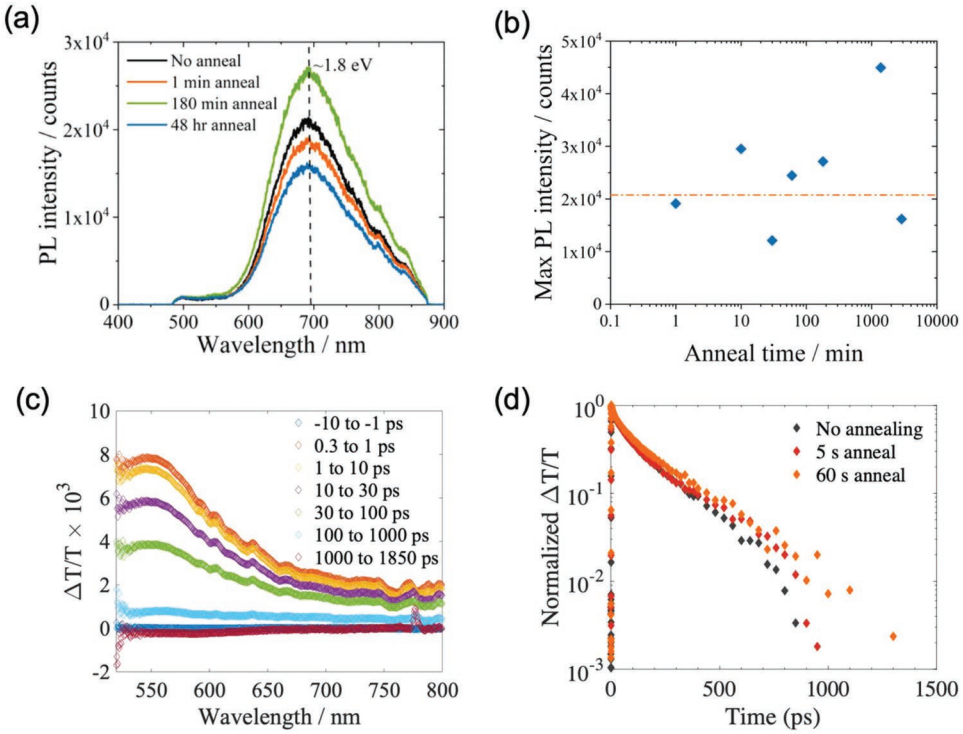

Figure 2. a) Photoluminescence (PL) spectra of as-deposited BiOI and vacuum annealed films. The full set of PL spectra is shown in Figure S4 (Supporting Information). b) Maximum photoluminescence intensity (at $\lambda = 692$ nm) for BiOI samples annealed under vacuum (100 °C, 25 Pa) for up to 48 h. The orange dashed line represents the maximum photoluminescence intensity before annealing. c) Transient absorption spectrum of nonannealed BiOI sample using a pump energy of 3.1 eV (400 nm) at a fluence of 136 μJ cm^{-2}. d) Integrated ground state bleach signal between 1.55 and 2.34 eV over time, showing the decay of carrier population.

electronic structure of BiOI occurred even when the I content halved, Bi content reduced by 20%, and O content more than doubled (Figure 1).

We next investigated the effect of compositional changes on the optoelectronic properties of BiOI. There was no shift in the PL peak position (selection of PL spectra shown in **Figure 2**a, with the spectra of all samples shown in Figure S4, Supporting Information). In addition, we did not observe a significant decrease in PL intensity with vacuum annealing (Figure 2b). All samples were measured in the same way using identical conditions (refer to the Experimental Section). This indicates that there was no change in bandgap and is consistent with no increase in nonradiative recombination across the vacuum annealing series.

Sister samples were grown onto cover slips without nickel oxide for measurements of the evolution of the charge carrier population with time after photoexcitation. Charge-carrier lifetimes were extracted from these measurements. When pumped at 400 nm, the transient absorption spectrum of the nonannealed sample exhibited a broad ground-state bleach (GSB) signal centered around 540 nm, due to the occupation of the bands by photoexcited charge carriers (Figure 2c). The breadth of the feature indicates that many optical transitions were blocked, most likely due to the flatness of the dispersion relation, which allowed the carriers at the band edge to occupy many different states in momentum space.

In order to track the decay of the carriers, the area under the GSB from 530 to 800 nm (1.55 to 2.34 eV) was measured at various times after excitation (Figure 2d). The resulting GSB kinetics exhibited an initial fast decay due to carrier-carrier annihilation, followed by a slower decay. The two decay regions may be due to a combination of surface and bulk recombination occurring. A biexponential model was fit to numerically describe the decay in GSB (**Table 1**). We focused our measurements on samples with up to 1 min vacuum annealing, in which the largest change in composition occurred (Figure 1a). The lifetime values in Table 1 show there to be no significant change in charge-carrier lifetime in BiOI films with up to 1 min vacuum annealing.

The transient absorption spectroscopy measurements were performed with a 400 nm wavelength laser, for which the absorption depth was ≈200 nm.[38] This raises the question of how far the surface composition changes measured by XPS are reflective of changes to the bulk composition. We performed

Table 1. Lifetime obtained by fitting a biexponential model to the normalized decay in the ground state bleach of BiOI films ($I(t)$) measured by transient absorption spectroscopy. The model used was $I(t) = A_1 e^{-\frac{t}{\tau_1}} + A_2 e^{-\frac{t}{\tau_2}}$.

Anneal time [s]	A_1	τ_1 [ps]	A_2	τ_2 [ps]
0	0.28	19	0.66	180
5	0.38	28	0.59	210
60	0.30	23	0.66	220

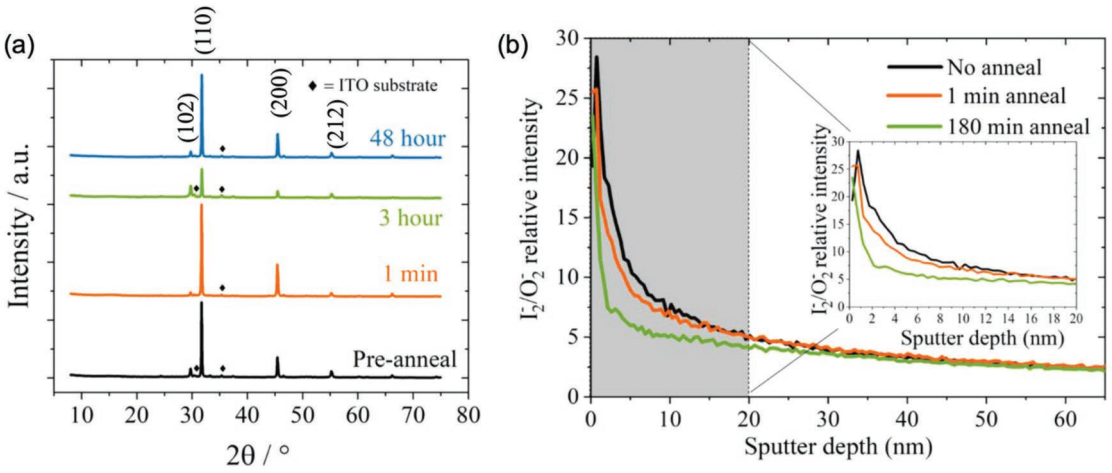

Figure 3. a) X-ray diffraction patterns of BiOI thin films grown on glass/ITO/NiO_x. The ♦ represents peaks from the ITO substrate. b) TOF-SIMS profile of I_2^- ion relative to O_2^- species for nonannealed, 1 and 180 min annealed samples. The inset includes the magnified profile for the first 20 nm of the surface.

X-ray diffraction measurements to determine whether changes to the bulk of the samples occurred. These measurements showed the films to remain in the tetragonal phase after vacuum annealing, with no peaks due to phase impurities appearing (**Figure 3**a). The diffraction peak positions also remained unchanged, showing there to be no change in lattice parameter. It is therefore likely that the changes in composition were mostly confined to the surface, such that the composition in the bulk was not affected.

To determine the depth to which the film composition was influenced by vacuum annealing, we performed energy-dispersive X-ray spectrometry (EDX) and time-of-flight secondary ion mass spectrometry (ToF-SIMS) measurements. We performed EDX measurements on the nonannealed and 10 min annealed sample (Table S1, Supporting Information). Five regions (5×3 μm^2) for each sample were measured. The interaction depth of the measurements was ≈300 nm (as determined from Monte Carlo simulations using the CASINO[44] program with an acceleration voltage of 12 keV). EDX measurements therefore probed a similar depth of the samples as our transient absorption spectroscopy measurements. We found the I/Bi ratio to be 0.973 ± 0.011 for the nonannealed sample and 0.971 ± 0.029 for the 10 min annealed sample. While the ratio of the annealed sample was marginally lower, indicating a reduction in the overall content of I, the change was within the error of the measurement. This case is plausible if we consider that the overall X-ray signals were collected from an interaction volume 300 nm deep, while the I fraction only decreased at the surface. EDX measurements were therefore consistent with the X-ray diffraction measurements in indicating that only the surface region of the BiOI film was affected by vacuum annealing and that the bulk of the samples were unaltered.

To further investigate the chemistry from the surface to the bulk of the nonannealed and vacuum-annealed films, SIMS depth profiling was carried out using a dual beam ToF-SIMS instrument. A Bi^+ primary ion beam and an Ar^+ sputter beam were utilized together to sputter through and obtain the composition of the ≈700 nm thick films. Figure 3b is the plot of the I_2^-/O_2^- ratio as a function of sputter depth and shows a clear trend in the I_2^-/O_2^- intensity dropping at a higher rate with increased annealing time. This is consistent with the XPS data. However, the rapid change in the ratio is not linearly correlated with the decrease in iodine content with annealing. The steeper declines in the I_2^-/O_2^- ratio for the annealed samples are a convoluted effect of a decrease in iodine content, increase in oxygen content, and preferential sputtering of oxygen during the depth profiling (this is demonstrated by the IO_2^- profiles measured in all samples, as shown in Figure S3, Supporting Information). The inset of Figure 3b shows the magnified I_2^-/O_2^- profiles of the samples. The initial increase in the intensity for the nonannealed and 1 min annealed samples in the inset of Figure 3b can be attributed to SIMS artifacts associated with the sputtering ion beam. The top ≈2 nm of the films were affected by pre-equilibrium effects which mask the true profiles of the region. However, the key point to note is that the vacuum annealing, even for prolonged periods, only altered the surface chemistry of the films and did not affect the bulk. This is evident by the I_2^-/O_2^- ratio leveling off at ≈40 nm of the sputtering depth with the fastest drop in intensity within the first 10 nm of the films.

The tens of nanometer region at the surface that iodine was removed from is substantially smaller than the absorption depth of the transient absorption spectroscopy measurements. The change in surface composition would therefore mostly affect the surface recombination measured in the GSB kinetics. Figure 2d shows that there was no significant change in the entire GSB profile with surface composition. These results therefore suggest the charge-carrier lifetime of BiOI to not be affected by substantial reductions in iodine content or increases in oxygen content. In addition, the PL measurements were taken with the same pump laser used for transient absorption measurements, and the emission would have mostly been from carriers recombining from the surface 200 nm region of the films. If any of the changes in composition induced mostly in the surface 10 nm led to active recombination centers, quenching of the PL would be expected. But this was found

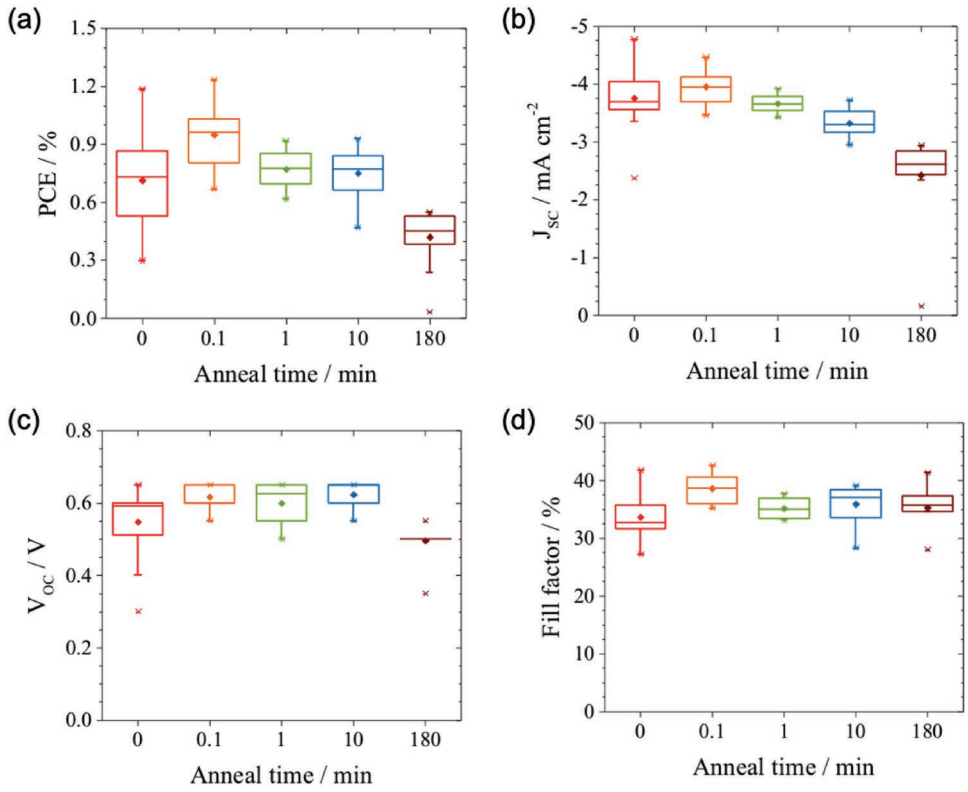

Figure 4. Performance of vacuum annealed BiOI thin films in photovoltaic devices. a) Power conversion efficiency (PCE), b) short-circuit current density (J_{sc}), c) open-circuit voltage (V_{OC}), and d) fill factor.

to not be the case. Thus, both the transient absorption and PL measurements are in agreement with our previous defect calculations of BiOI, which showed the transition levels for iodine vacancies and oxygen-on-iodine antisite defects to be resonant within the conduction and valence bands, respectively, and not recombination active.[38]

Finally, we investigated the effect of vacuum annealing on the performance of the BiOI films in photovoltaic devices. The device structure was ITO/NiO_x/BiOI/ZnO/Cr/Ag (refer to ref. [38] for the band structure of BiOI and the device stack). **Figure 4**a shows there to be no significant change in the power conversion efficiency (PCE) with annealing time compared to the reference (labeled as 0 min anneal time). The device with 180 min annealed BiOI had a lower median PCE, but the distribution of PCEs overlapped with those of the other samples. While the short-circuit current densities of these devices were statistically significantly lower than the control (Figure 4b), the open-circuit voltages and fill factors were not significantly different. We note that the BiOI films used for vacuum annealing at 180 min did not have optimal morphology to start with, and the lower median short-circuit current density may not have been solely due to changes in surface composition. The shunt resistances of the devices across different annealing times also remained at an average value of 350 ± 30 Ω cm^2. This suggests that there is no significant increase in nonradiative recombination in the devices with increasing vacuum annealing.

The robustness of the performance of BiOI against percent-level changes in surface composition is highly advantageous for the processing of devices using facile methods. We previously found the surface I/Bi ratio to decrease from 1.0 (as-grown BiOI film) to 0.6 after depositing the ZnO electron transport layer. This is similar to the effect of vacuum annealing BiOI for 1 min. Depositing ZnO over BiOI thin films that have already been vacuum annealed may have further reduced the I content relative to the Bi content, but this evidently did not have an impact on the device performance. Indeed, our results show BiOI to be significantly tolerant to changes in the surface iodine content, which may afford greater flexibility in how the electron transport layer is grown on top.

3. Discussion

Our results show that BiOI tolerates significant changes in the composition of iodine, oxygen, and bismuth at the surface. The lifetime and PL intensity were unaffected, suggesting that no extra deep recombination centers were introduced by the changes in composition. BiOI also appears to be electronically tolerant to the compositional changes, with the Bi $4f_{7/2}$ core level not significantly changing in binding energy, and the valence band density of states also remaining the same shape over the entire vacuum annealing series.

The reduction in iodine and bismuth content is likely due to the formation of iodine (V_I) and bismuth vacancies (V_{Bi}), which are two of the lowest formation energy defects in BiOI. Our previous calculations showed these defects to have transition levels that are resonant within the conduction band (V_I) or shallow in the bandgap (V_{Bi}),[38] and our experimental results are consistent

with this. The increase in the surface oxygen content could have been due to three possibilities: 1) the formation of oxygen-on-iodine antisite defects (O_I), 2) removal of the surface layers of iodine and bismuth to expose the oxygen layer of BiOI to the surface, or 3) the formation of different phases on the surface.

The first possibility is likely because our previous calculations showed O_I to have similarly low formation energies as V_I and V_{Bi}. This is expected because I^- has a larger ionic radius than O^{2-},[45] and it would not be difficult for O^{2-} to fill an empty I^- site. O_I is also predicted to have no transition level within the bandgap of BiOI,[38] which is consistent with our measurements showing the optoelectronic properties and electronic structure of BiOI to be robust to increases in O content. The second possibility is also likely given that oxygen vacancies (V_O) have a higher formation energy than V_I and V_{Bi},[38] showing it to be less thermodynamically favorable to remove O from the lattice than it is to remove I or Bi. This is supported by thermogravimetric analyses of BiOI by Klimakov et al., who showed that only BiI^+, Bi^+, I_2^+, and BiI_2^+ ions were removed when BiOI was heated at 100 to 250 °C.[46]

To investigate the third possibility, we analyzed the O 1s core level spectra of BiOI thin films annealed for different times (Figure S5, Supporting Information). We found there to be three peaks, located at binding energies of 529, 531, and 533 eV. With increased vacuum annealing, the contribution of the peaks at 531 and 533 eV to the overall O 1s spectra increased (Figure S6, Supporting Information). The peak at 529 eV binding energy could be attributed to lattice oxygen in BiOI. But the origin of the peaks at binding energies of 531 and 533 eV is not well documented. Previous reports have attributed these to adsorbed organic contaminants or moisture,[47,48] or other oxide/oxyhalide species (e.g., Bi_2O_3 or Bi_5O_7I).[49,50] The first option is not likely because the BiOI films were annealed under vacuum, and it is unlikely that water or organic contaminants could have adsorbed to the surface more with longer vacuum annealing. The BiOI samples were transferred immediately to the XPS vacuum load lock after growth. To investigate the second possibility, we grew three samples with different mixed phases (detailed in Table S2, Supporting Information). However, sample A (with a mixture of BiOI and Bi_5O_7I phases) had a Fermi level to valence band offset that was significantly different to the values measured for the vacuum annealed BiOI samples (Table S3, Supporting Information). For samples B and C, the valence band XPS spectra had a significantly different shape to those of BiOI and vacuum-annealed BiOI (Figure S7, Supporting Information). In all three mixed-phase samples, the fractions of each element were significantly different to the fractions measured in the vacuum-annealed BiOI (Figure S8, Supporting Information), and the Bi $4f_{7/2}$ core level peaks also had different binding energies to BiOI (Figure S9, Supporting Information). These results all suggest that it is unlikely that the O 1s peaks at 531 and 533 eV binding energy were due to the formation of mixed phases on the surface of vacuum-annealed BiOI. It is possible that these O 1s core level peaks could have been due to the different bonding environment for O^{2-} when it occupies a lattice I^- site (as O_I) or when the oxygen layer is on the surface of BiOI. Similarly, although the full-width at half maximum (FWHM) of the Bi $4f_{7/2}$ core level peaks for vacuum-annealed films was wider than the FWHM for as-grown BiOI (1.02 eV, compared to 0.92 eV; Figure 1c), this was likely due to the different bonding environment for Bi^{3+} in the presence of percent-level defects. There was no increase in FWHM with increasing annealing time, which further suggests that no second phases or any stabilizing surface layer formed. Overall, the increase in the fraction of surface oxygen observed in Figure 1a is likely due to a combination of the first two possibilities, which may have been why the rate of surface oxygen content increase was greater than the rate of decrease in the surface iodine content (Figure 1b).

The Fermi level of the vacuum-annealed BiOI films remained close to mid-gap, even after 48 h vacuum annealing. A plausible explanation for this observation is self-compensation in BiOI. Previous theoretical analyses have shown that self-compensation occurs in materials when the concentration of defects is higher than the concentration of thermally excited carriers from the band edges.[25] The Fermi level position is then controlled by the lowest formation-energy donor and acceptor defects, and will be "pinned" to the energy at which these defects have the same formation energy. This is because if the Fermi level shifts to a higher energy (i.e., closer to the conduction band minimum), the acceptor defect then has a lower formation energy than the donor defect. The resulting higher concentration of holes than electrons leads to the Fermi level returning back to the original position. Similar arguments can be made if the Fermi level moves to lower energies. An important consequence of Fermi level pinning is that donor and acceptor defects with the same charge have the same concentration because they have the same formation energy. Thus, despite high concentrations of these defects, the semiconductor will maintain low carrier concentrations because the defects are charge-compensated.[9,24,25] Our results strongly suggest self-compensation occurs in BiOI. First, the percent-level concentration of V_I, O_I, and V_{Bi} defects measured experimentally would be larger than the thermally excited density of carriers in BiOI. Also, our previous defect calculations showed V_I, O_I, and V_{Bi} to all have low formation energies (V_I and O_I in particular have low formation energies across all Fermi energies).[38] This agrees with our measurements showing that the concentration of iodine, bismuth, and oxygen change easily with vacuum annealing (Figure 1a). In particular, our previous calculations showed that the donor and acceptor defects intersect at a formation energy of ≈0.5 eV or below, depending on the chemical potentials.[38] This is likely lower than the formation energies associated with the thermally excited carriers at the same Fermi energy. The Fermi level of BiOI is therefore most likely determined by its defects. Furthermore, our previous calculations showed that the Fermi energy at which the donor and acceptor defects intersect is close to mid-gap,[38] which agrees with the XPS measurements (Figure 1d). In BiOI, the lowest formation energy donor defect is V_I, and the lowest formation energy acceptor defect either O_I or V_{Bi}.[38] Our measurements in Figure 1a show that the initial changes in oxygen and iodine content were approximately similar, suggesting that O_I accompanying the formation of V_I is plausible (as discussed before). Figure 1a also shows that the overall reduction in bismuth content is approximately one-third the overall reduction in iodine content, and it is also plausible that each V_{Bi} is accompanied by three V_I. Either case would result in charge compensation, since O_I has the same absolute charge as V_I (unity), and the absolute

charge of V_{Bi} is three times that of V_I. This is consistent with the carrier concentration of BiOI remaining low (and the Fermi level being mid-gap across the entire vacuum annealing series) despite these defects being present at the percent-level.

Finally, we aim to understand why the bulk lifetimes of the BiOI thin films measured by transient absorption spectroscopy are short (Table 1). We hypothesize that while BiOI is tolerant toward V_I, O_I, and V_{Bi}, deep traps are present in the as-grown samples which lead to high rates of nonradiative recombination. To experimentally determine whether or not deep traps are present, we performed photoinduced current transient spectroscopy (PICTS). PICTS is a deep-level characterization technique similar to the more widely known deep-level transient spectroscopy (DLTS). While DLTS relies on trap filling at the edge of a depletion region via carriers sourced by the semiconductor bulk (therefore suitable for characterizing doped semiconductors), PICTS is the technique of choice for near-intrinsic/highly resistive semiconductors, such as BiOI.[51–54] Indeed, PICTS involves trap filling via photogenerated carriers under pulsed illumination, and it allows one to determine deep-level parameters (energy depth with respect to either band edge, capture cross section, and volumetric density) from the current decay (which relates to carrier emission from the deep levels) resulting from the light pulses. We performed PICTS measured on BiOI solar cells, fabricated as detailed earlier, and subjected to vacuum annealing for 0 min (i.e., no annealing), 1 min, and 180 min. The PICTS measurements were conducted at over a temperature range of 160–300 K under pulsed illumination at a wavelength of 617 nm. The resulting PICTS spectra and Arrhenius plots of the associated peaks are shown in Figures S11 and S12 (Supporting Information).

From the PICTS measurements, we identified two main deep levels, which we labeled as P1 and P2. The deep-level energies and volumetric concentrations for all samples are shown in **Figure 5**. P1 was shallower than P2, but both had similar volumetric densities on the order of 10^{16}–10^{17} cm^{-3} (under the assumption of uniform distribution in the volume of the BiOI films). This shows deep levels are indeed present, even in the as-grown films. We estimated their capture cross sections from the extrapolation of the Arrhenius plots, consistently with basic emission rate modeling (involving, among others, the assumption that capture cross sections are temperature-independent). We found the capture cross sections to be small for P1 (10^{-15}–10^{-14} cm^2) but large for P2 (10^{-12}–10^{-11} cm^2),[16] indicating P2 to be particularly recombination active (Figure S10, Supporting Information). The capture cross section for P2 is larger than the capture cross section for deep defects found in LHPs (0.76 eV from a band edge). The capture cross section for these deep traps was only 10^{-14} cm^2 and 18%-efficient LHP solar cells were still achievable.[16]

We considered the possibility that P1 or P2 could be due to the V_I, O_I, or V_{Bi} induced by vacuum annealing. This is unlikely because our results show P1 and P2 to be present in the as-grown BiOI thin film. Even though we halve the I fraction and more than double the O fraction on the surface, there is no significant change in the concentration of P1 or P2 after 1 or 180 min vacuum annealing (Figure 5b). If we remove half of the I from the surface 10 nm of BiOI (ToF-SIMS in Figure 3b shows that we are mostly removing I from the top 10 nm of the BiOI film), then over the entire 700 nm thickness of BiOI, the V_I concentration would average to be 10^{20} cm^{-3}, which is three to four orders of magnitude larger than the concentration of P1 or P2. Hence, P1 and P2 are unlikely to be V_I, and similar arguments can be applied to O_I and V_{Bi}. If the trap density were on the order of 10^{20} cm^{-3}, the Shockley–Read–Hall recombination lifetime would be below the picosecond timescale, far shorter than the lifetimes measured.[55] The trap levels for V_I, V_{Bi}, and O_I would not be detectable if their transition levels were resonant within the bands or <0.1 eV from the band edges (owing to our measurements only going down to 160 K), as predicted from our previous calculations.[38] Thus, it is likely that the deep traps detected by PICTS are not due to the changes in surface composition we induced through vacuum annealing and that BiOI does indeed tolerate significant levels of V_I, V_{Bi}, and O_I. We postulate that P1 and P2 may originate from 1) oxygen vacancies, which may have been formed during kinetically driven growth conditions despite them thermodynamically having high formation energies,[56,57] 2) interstitial defects or defect complexes that were not considered in the previous calculations,[38] 3) extrinsic impurities being present, or 4) traps introduced by structural defects. Future work will need to focus on identifying the origin of these traps.

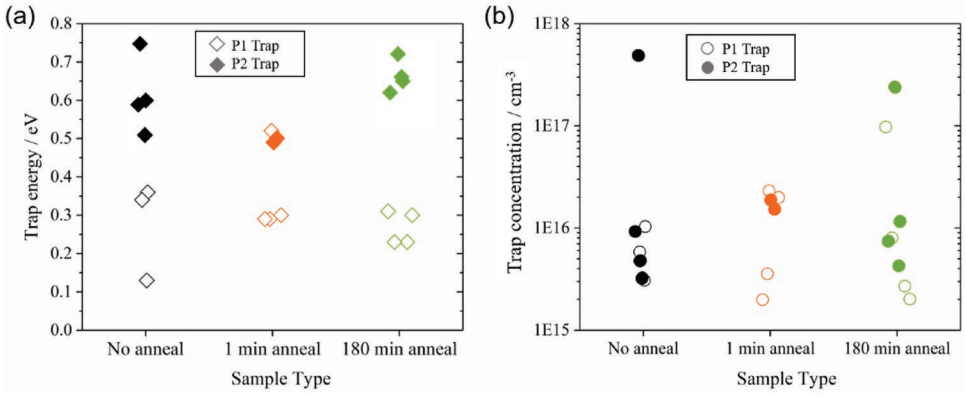

Figure 5. PICTS data for vacuum annealed samples. a) Trap energy levels and b) trap concentration of nonannealed, 1 min annealed, and 180 min annealed samples. Two traps were found in the PICTS spectra and these are labeled P1 and P2 (refer to Figures S11 and S12, Supporting Information, for more details). The open points are for the P1 trap found in each sample, while the closed points are for the P2 trap in each sample.

We also note that an alternative explanation for the invariance of the Fermi level with vacuum annealing is that the Fermi level is pinned due to high defect concentrations. But apart from V_I, O_I, and V_{Bi}, which do not have deep transition levels, the only defects we found are P1 and P2. If the Fermi level is pinned by P1 or P2, we would not expect the Fermi level to be mid-gap. Also, the concentrations of P1 and P2 are orders of magnitude smaller than V_I, O_I, and V_{Bi}, and we would expect these latter defects to more strongly influence the Fermi level position, as discussed before.

4. Conclusion

In summary, we have experimentally found BiOI to be electronically and optoelectronically robust against percent-level changes in the surface content of iodine, bismuth, and oxygen. This agrees with our previous defect calculations. The extent of tolerance to these point defects is greater than the tolerance of $MAPbI_3$ to V_I and V_{MA}, in which the Fermi level and Pb $4f_{7/2}$ core level shifted when I/Pb decreased below 2.5. By contrast, we observed no shift in Fermi level or Bi $4f_{7/2}$ core level even when the I and Bi fractions reduced by 50% and 20%, respectively, and the O fraction increased by 80% after 2 d of vacuum annealing. We attribute these observations to self-compensation between the lowest formation energy donor (V_I) and acceptor (either O_I or V_{Bi}) defects. There was also no significant change in the photoluminescence intensity after 2 d vacuum annealing, suggesting that no extra nonradiative recombination centers were introduced. Transient absorption spectroscopy showed that there was no significant change in the charge-carrier lifetime in the BiOI films after 1 min vacuum annealing, when the I fraction had been reduced by 40%, Bi fraction reduced by 5%, and O fraction increased by 45%. The photovoltaic performance of these films was also not significantly degraded indicating tolerance to these defects. However, PICTS measurements showed deep traps to be present ≈0.3 and 0.6 eV from the band edge. These traps were present in the as-grown films and did not increase in concentration with vacuum annealing. Their concentrations were also three to four orders magnitude lower than the expected concentration of the V_I, V_{Bi}, and O_I traps induced through vacuum annealing and it is likely that the traps found from the PICTS measurements were of a different origin. Our work supports theoretical predictions that BiOI tolerates V_I, V_{Bi}, and O_I. This result motivates future efforts to develop BiOI photovoltaics further, showing the important direction to be followed, namely, by identifying the deep traps present in as-grown films and developing protocols to overcome them. Our work suggests that the reward for these efforts would be a boost in efficiency in a material that is robust to processing conditions that give rise to percent-level concentrations of point defects, and therefore compatible with low-cost fabrication methods.

5. Experimental Section

Thin Film Synthesis: Glass substrates were sequentially cleaned in acetone (Fisher Scientific, >99.8%) and propan-2-ol (Fisher Scientific, >99.5%) for 15 min each by ultrasonication. The substrates were subsequently dried with compressed air and plasma treated (Zepto, Diener) for 10 min.

The substrates were then covered with a 10 nm thin film of NiO_x using previously reported recipe.[38] The Ni sol was prepared by mixing 1 mol L^{-1} nickel nitrate hexahydrate (Sigma Aldrich) in ethylene glycol (Sigma Aldrich) and adding 1 mol L^{-1} ethylenediamine (Sigma Aldrich). This sol was filtered with a 0.22 µm PTFE filter. A droplet of the filtered sol was pushed through another 0.22 µm PTFE filter and spread over the plasma-cleaned substrate. This was spin-coated at 5000 rpm for 45 s and annealed in air on a hotplate (Stuart UC152D). The set temperatures of the hotplate were 125 °C (40 min) and 300 °C (70 min). The films were subsequently quenched on Al foil and immediately stored in a dry cabinet (0.1% relative humidity, Superdry-Totech).

BiOI thin films were grown by chemical vapor deposition at atmospheric pressure following a previously reported method.[38] A two-zone furnace with a quartz tube was used. The furnace was preheated to 350 °C in zones 1 and 2. Four substrates were attached to a microscope slide using silver paste (Electrolube) and loaded into the tube. 500 mg of BiI_3 (Alfa Aesar Puratronic, 99.999% metals basis) was weighed into a crucible and placed close to the edge of the heating rod in zone 1 of the furnace. The substrates were at least 3 cm away from the center of the crucible. An $Ar:O_2$ gas mixture (25 mL min^{-1} Ar, 0.3 mL min^{-1} O_2) was introduced into the closed tube. Each growth run lasted for 60 min, which resulted in BiOI films that were ≈700 nm thick.

Characterization: X-ray photoemission spectroscopy was performed using a SPECS PHOIBOS 150 electron energy analyzer. Monochromated Al $K_{\alpha 1}$ X-rays (1486.6 eV photon energy) were used as the photon source. The energy resolution was 0.50 eV. The binding energy scale was calibrated to the C 1s core level at 284.4 eV for adventitious carbon.

Photoluminescence spectra were measured using an intensified charge-coupled device camera (Andor iStar DH740 CCI-010 connected to a grating spectrometer (Andor SR303i). The samples were excited in ambient air using a 400 nm wavelength laser. This laser was frequency-doubled from a Ti:Sapphire laser (Spectra Physics Solstice) that had a wavelength of 800 nm, repetition rate of 1 kHz, and pulse length of ≈90 fs. An exposure time of 0.2 s and gate width of 400 µm was used. The fluence used was 760 µJ cm^{-2} $pulse^{-1}$. Ten accumulations were used for each spectra.

Transient absorption spectroscopy measurements were performed using the same laser source as the photoluminescence measurements. The source laser was also frequency-doubled to give a 400 nm wavelength pump beam. To generate a broadband (500–800 nm wavelength), a home-built noncollinear optical parametric amplifier was used. The sample was aligned such that the pump and probe beams overlapped. Adjacent to these was a reference probe beam to account for shot-to-shot variation in probe transmission through the sample. The imaging spectrometer was an Andor Shamrock SR303i and the detector a pair of linear image sensors (Hamamatsu, G11608). To determine the differential transmittance ($\Delta T/T$), a mechanical/electronic chopper to create the "pump on" and "pump off" periods for each measurement, detected with a lock-in amplifier, was used. More details are reported in ref. [58].

EDX measurements were taken on a FEI Nova NanoSEM at a base pressure of 10^{-5} mbar. The acceleration voltage of the electron beam was 12 kV, such that the incident energy was sufficient to excite the core level electrons in Bi and I. Prior to performing the EDX measurements, a copper reference sample to check the binding energy scale was used.

ToF-SIMS measurements were taken using an IONTOF ToF-SIMS V instrument. A 25 keV Bi^+ primary ion beam was rastered over the BiOI film to determine the mass spectra, over an analytical area of 100 μm^2. A 500 eV Ar^+ ion beam was used to sputter the film with a current of ≈40 nA over an area of 300 μm^2. Negative secondary ions were collected.

PICTS experiments were conducted on solar cell samples placed in a liquid-He cryostat, whose temperature was varied from 160 and 300 K with a heating rate of 1 K min^{-1}. The optical and electrical acquisition units were custom-built, were controlled via LabVIEW, and comprise a light-emitting diode with peak emission wavelength of 617 nm. The light pulse duration was set to 1 s throughout the

experiments. The recorded current waveforms were digitized and processed according to a boxcar-type algorithm,[59] which delivers the PICTS spectra presented in Figures S11 and S12 (Supporting Information). By fitting the peaks of these spectra with Gaussian functions, the emission rate was derived as a function of temperature of the corresponding deep levels, which were then analyzed through the Arrhenius plots presented in Figures S11 and S12 (Supporting Information). Such analysis delivered the energy depth of the deep levels within the forbidden gap and their capture cross sections (under the assumption of temperature independence of the latter).[60] Volumetric densities of the deep levels were extracted from the integrated current transients, under the assumption of uniform distribution throughout the bulk of the BiOI layer.

Device Fabrication and Testing: The device structure for BiOI was the same as that developed in a previous report, and the details can be found in ref. [38]. ZnO was deposited over the ITO/NiO_x/BiOI stack by atmospheric pressure chemical vapor deposition. Diethylzinc (Sigma Aldrich) was used as the Zn precursor and O_2 gas (Air Products, <3 ppm H_2O) was the oxidant. 20 nm Cr and 100 nm Ag were sequentially thermally evaporated (<1 nm s^{-1} rate; 7×10^{-6} mbar absolute base pressure) on top of the ZnO through a shadow mask. The device area is defined by the overlap between the Cr/Ag top electrode and the patterned ITO bottom electrode, and this was 4.5 mm^2 for each device.

The devices were characterized by illuminating with a calibrated AM 1.5G spectrum (ABET 2000). Current–voltage sweeps were made using a Keithley 2623A sourcemeter unit, at a rate of 1 V s^{-1}. The voltage was swept from −1 to 1.4 V with a step size of 0.05 V and delay of 0.05 s. It is noted that the devices were not apertured because it was previously found to not significantly affect the short-circuit current densities measured, which were consistent with the external quantum efficiency measurements.[38]

Supporting Information

Supporting Information is available from the Wiley Online Library or from the author. The raw data can be found on http://dx.doi.org/10.17863/CAM.48280.

Acknowledgements

T.N.H. acknowledges funding from the EPSRC Centre for Doctoral Training in Graphene Technology (No. EP/L016087/1) and the Aziz Foundation. L.C.L. acknowledges funding from the EPSRC Centre for Doctoral Training in New and Sustainable Photovoltaics. L.E. acknowledges funding from the EPSRC Centre for Doctoral Training in Nanoscience and Nanotechnology (EP/L015978/1). W.-W.L. and J.L.M.-D. acknowledge support from the EPSRC (Nos. EP/L011700/1 and EP/N004272/10), and the Isaac Newton Trust (Minute 13.38(k)). R.A.J. acknowledges funding from an EPSRC Department Training Partnership studentship (No. EP/N509620/1), as well as Bill Welland and the Winton Programme for the Physics of Sustainability. F.D. acknowledges funding from the DFG Emmy Noether Programme. V.P. is thankful for the support from the National Natural Science Foundation of China (61750110517, 61950410759, and 61805166), the Jiangsu Province Natural Science Foundation (BK20170345), the Collaborative Innovation Center of Suzhou Nano Science & Technology, the Priority Academic Program Development of Jiangsu Higher Education Institutions (PAPD), the 111 Project, and the Joint International Research Laboratory of Carbon-Based Functional Materials and Devices. R.L.Z.H. acknowledges support from the Royal Academy of Engineering under the Research Fellowship scheme (No. RF\201718\1701), the Isaac Newton Trust (Minute 19.07(d)), and the Kim and Juliana Silverman Research Fellowship at Downing College, Cambridge. The authors also acknowledge financial support from EPSRC Grant No. EP/P027032/1.

Conflict of Interest

The authors declare no conflict of interest.

Author Contributions

T.N.H. and L.C.L. contributed equally to this work. T.N.H. fabricated and vacuumed annealed BiOI thin films for transient absorption, ToF-SIMs, EDX and PICTS measurements, along with the fabrication and measurement of the photovoltaic devices. L.C.L. carried out the initial fabrication and annealing of the thin films for XPS, XRD and PL measurements, along with the fabrication and analysis of mixed-phased BiOI samples. L.E. performed the transient absorption spectroscopy measurements. R.A.J. performed the EDX measurements. W.-W.L. carried out the XPS measurements. C.K. and V.P. performed the PICTS measurements. S.F. performed the ToF-SIMS measurements and analysis. R.L.Z.H. conceived of the project, helped to plan the experiments, performed the PL measurements and guided the analysis. All authors contributed to writing the paper and discussing the results.

Keywords

bismuth-based solar absorbers, defect tolerance, perovskite-inspired materials, photoinduced current transient spectroscopy, photovoltaics

Received: November 29, 2019
Revised: January 9, 2020
Published online: February 14, 2020

[1] NREL, "Best Research-Cell Efficiency Chart," can be found under https://www.nrel.gov/pv/assets/pdfs/best-research-cell-efficiencies.20190703.pdf (accessed: November 2019).
[2] J. J. Yoo, S. Wieghold, M. C. Sponseller, M. R. Chua, S. N. Bertram, N. T. P. Hartono, J. S. Tresback, E. C. Hansen, J. P. Correa-Baena, V. Bulović, T. Buonassisi, S. S. Shin, M. G. Bawendi, *Energy Environ. Sci.* **2019**, *12*, 2192.
[3] M. A. Green, A. Ho-Baillie, H. J. Snaith, *Nat. Photonics* **2014**, *8*, 506.
[4] P. K. Nayak, S. Mahesh, H. J. Snaith, D. Cahen, *Nat. Rev. Mater.* **2019**, *4*, 269.
[5] R. L. Z. Hoye, M. L. Lai, M. Anaya, Y. Tong, K. Gałkowski, T. Doherty, W. Li, T. N. Huq, S. Mackowski, L. Polavarapu, J. Feldmann, J. L. MacManus-Driscoll, R. H. Friend, A. S. Urban, S. D. Stranks, *ACS Energy Lett.* **2019**, *4*, 1181.
[6] A. Miyata, A. Mitioglu, P. Plochocka, O. Portugall, J. T. W. Wang, S. D. Stranks, H. J. Snaith, R. J. Nicholas, *Nat. Phys.* **2015**, *11*, 582.
[7] T. Kirchartz, L. Krückemeier, E. L. Unger, *APL Mater.* **2018**, *6*, 100702.
[8] D. Kiermasch, P. Rieder, K. Tvingstedt, A. Baumann, V. Dyakonov, *Sci. Rep.* **2016**, *6*, 39333.
[9] A. Walsh, D. O. Scanlon, S. Chen, X. G. Gong, S. H. Wei, *Angew. Chem., Int. Ed.* **2015**, *54*, 1791; *Angew. Chem.* **2015**, *127*, 1811.
[10] R. E. Brandt, J. R. Poindexter, R. C. Kurchin, P. Gorai, R. L. Z. Hoye, L. Nienhaus, M. W. B. Wilson, J. A. Polizzotti, R. Sereika, R. Žaltauskas, L. C. Lee, J. L. MacManus-Driscoll, M. Bawendi, V. Stevanović, T. Buonassisi, *Chem. Mater.* **2017**, *29*, 4667.
[11] J. R. Poindexter, R. L. Z. Hoye, L. Nienhaus, R. C. Kurchin, A. E. Morishige, E. E. Looney, A. Osherov, J. P. Correa-Baena, B. Lai, V. Bulović, V. Stevanović, M. G. Bawendi, T. Buonassisi, *ACS Nano* **2017**, *11*, 7101.

[12] M. T. Klug, A. Osherov, A. A. Haghighirad, S. D. Stranks, R. P. Brown, S. Bai, J. T.-W. Wang, X. Dang, V. Bulovic, H. J. Snaith, A. M. Belcher, *Energy Environ. Sci.* **2017**, *10*, 236.
[13] D. Meggiolaro, S. G. Motti, E. Mosconi, A. J. Barker, J. Ball, C. A. R. Perini, F. Deschler, A. Petrozza, F. De Angelis, *Energy Environ. Sci.* **2018**, *11*, 702.
[14] S. Sun, N. T. P. Hartono, Z. D. Ren, F. Oviedo, A. M. Buscemi, M. Layurova, D. X. Chen, T. Ogunfunmi, J. Thapa, S. Ramasamy, C. Settens, B. L. DeCost, A. G. Kusne, Z. Liu, S. I. P. Tian, I. M. Peters, J.-P. Correa-Baena, T. Buonassisi, *Joule* **2019**, *3*, 1437.
[15] W. S. Yang, B.-W. Park, E. H. Jung, N. J. Jeon, Y. C. Kim, D. U. Lee, S. S. Shin, J. Seo, E. K. Kim, J. H. Noh, S. Il Seok, *Science* **2017**, *356*, 1376.
[16] Y. Lee, M. Khaja, S. Heo, G. Seo, D. Lee, M. Seol, J. Lee, J.-B. Park, K. Kim, D.-J. Yun, Y. S. Kim, J. K. Shin, T. K. Ahn, M. K. Nazeeruddin, *Energy Environ. Sci.* **2017**, *10*, 1128.
[17] L. C. Lee, T. N. Huq, J. L. MacManus-Driscoll, R. L. Z. Hoye, *APL Mater.* **2018**, *6*, 084502.
[18] X. Wen, Y. Feng, S. Huang, F. Huang, Y.-B. Cheng, M. Green, A. Ho-Baillie, *J. Mater. Chem. C* **2016**, *4*, 793.
[19] S. D. Stranks, *ACS Energy Lett.* **2017**, *2*, 1515.
[20] H. Jin, E. Debroye, M. Keshavarz, I. G. Scheblykin, M. B. J. Roeffaers, J. Hofkens, J. A. Steele, *Mater. Horiz.* **2020**.
[21] S. D. Stranks, V. M. Burlakov, T. Leijtens, J. M. Ball, A. Goriely, H. J. Snaith, *Phys. Rev. Appl.* **2014**, *2*, 034007.
[22] B. Zhao, L. C. Lee, L. Yang, A. J. Pearson, H. Lu, X. J. She, L. Cui, K. H. L. Zhang, R. L. Z. Hoye, A. Karani, P. Xu, A. Sadhanala, N. C. Greenham, R. H. Friend, J. L. MacManus-Driscoll, D. Di, *ACS Appl. Mater. Interfaces* **2018**, *10*, 41849.
[23] S. Ahmad, A. Sadhanala, R. L. Z. Hoye, V. Andrei, M. H. Modarres, B. Zhao, J. Rongé, R. Richard, M. De Volder, *ACS Appl. Mater. Interfaces* **2019**, *11*, 23198.
[24] K. X. Steirer, P. Schulz, G. Teeter, V. Stevanovic, M. Yang, K. Zhu, J. J. Berry, *ACS Energy Lett.* **2016**, *1*, 360.
[25] J. H. Yang, W. J. Yin, J. S. Park, S. H. Wei, *Sci. Rep.* **2015**, *5*, 1.
[26] M. Jahandar, N. Khan, H. K. Lee, S. K. Lee, W. S. Shin, J.-C. Lee, C. E. Song, S.-J. Moon, *ACS Appl. Mater. Interfaces* **2017**, *9*, 35871.
[27] S. B. Zhang, S.-H. Wei, A. Zunger, *Phys. Rev. Lett.* **1997**, *78*, 40594.
[28] M. Stutzmann, *Philos. Mag. B* **1989**, *60*, 531.
[29] A. Babayigit, A. Ethirajan, M. Muller, B. Conings, *Nat. Mater.* **2016**, *15*, 247.
[30] A. Babayigit, D. D. Thanh, A. Ethirajan, J. Manca, M. Muller, H. G. Boyen, B. Conings, *Sci. Rep.* **2016**, *6*, 18721.
[31] U.S. Geological Survey, *Mineral Commodity Summaries* **2019**, *2019*.
[32] R. E. Brandt, V. Stevanović, D. S. Ginley, T. Buonassisi, *MRS Commun.* **2015**, *5*, 265.
[33] R. C. Kurchin, P. Gorai, T. Buonassisi, V. Stevanović, *Chem. Mater.* **2018**, *30*, 5583.
[34] A. M. Ganose, C. N. Savory, D. O. Scanlon, *Chem. Commun.* **2017**, *53*, 20.
[35] J. P. Correa-Baena, L. Nienhaus, R. C. Kurchin, S. S. Shin, S. Wieghold, N. T. P. Hartono, M. Layurova, N. D. Klein, J. R. Poindexter, A. Polizzotti, S. Sun, M. G. Bawendi, T. Buonassisi, *Chem. Mater.* **2018**, *30*, 3734.
[36] R. L. Z. Hoye, R. E. Brandt, A. Osherov, V. Stevanovic, S. D. Stranks, M. W. B. Wilson, H. Kim, A. J. Akey, J. D. Perkins, R. C. Kurchin, J. R. Poindexter, E. N. Wang, M. G. Bawendi, V. Bulovic, T. Buonassisi, *Chem. - Eur. J.* **2016**, *22*, 2605.
[37] R. Mohan, *Nat. Chem.* **2010**, *2*, 336.
[38] R. L. Z. Hoye, L. C. Lee, R. C. Kurchin, T. N. Huq, K. H. L. Zhang, M. Sponseller, L. Nienhaus, R. E. Brandt, J. Jean, J. A. Polizzotti, A. Kursumović, M. G. Bawendi, V. Bulović, V. Stevanović, T. Buonassisi, J. L. MacManus-Driscoll, *Adv. Mater.* **2017**, *29*, 1702176.
[39] N. J. Podraza, W. Qiu, B. B. Hinojosa, H. Xu, M. A. Motyka, S. R. Phillpot, J. E. Baciak, S. Trolier-Mckinstry, J. C. Nino, *J. Appl. Phys.* **2013**, *114*, 033110.
[40] D. Tiwari, D. Alibhai, D. J. Fermin, *ACS Energy Lett.* **2018**, *3*, 1882.
[41] B. Yoo, D. Ding, J. M. Marin-Beloqui, L. Lanzetta, X. Bu, T. Rath, S. A. Haque, *ACS Appl. Energy Mater.* **2019**, *2*, 7056.
[42] R. Jaramillo, M. J. Sher, B. K. Ofori-Okai, V. Steinmann, C. Yang, K. Hartman, K. A. Nelson, A. M. Lindenberg, R. G. Gordon, T. Buonassisi, *J. Appl. Phys.* **2016**, *119*, 035101.
[43] M. Schmidt, H. Oppermann, H. Brucner, Z. Binnewies*Z. Anorg. Allg. Chem.* **1997**, *623*, 1945.
[44] P. Hovington, D. Drouin, R. Gauvin, *Scanning* **1997**, *19*, 1.
[45] R. D. Shannon, *Acta Crystallogr., Sect. A: Found. Adv.* **1976**, *32*, 751.
[46] A. M. Klimakov, B. A. Popovkin, A. Novoselova, *Russ. J. Inorg. Chem.* **1974**, *19*, 1394.
[47] N. T. Hahn, S. Hoang, J. L. Self, C. B. Mullins, *ACS Nano* **2012**, *6*, 7712.
[48] D. S. Bhachu, S. J. A. Moniz, S. Sathasivam, D. O. Scanlon, A. Walsh, S. M. Bawaked, M. Mokhtar, A. Y. Obaid, I. P. Parkin, J. Tang, C. J. Carmalt, *Chem. Sci.* **2016**, *7*, 4832.
[49] X. Jiang, Y. Ma, C. Zhao, Y. Chen, M. Cui, J. Yu, Y. Wu, Y. He, *J. Mater. Res.* **2018**, *33*, 2385.
[50] A. Walsh, G. W. Watson, D. J. Payne, R. G. Edgell, J. Guo, P.-A. Glans, T. Learmonth, K. E. Smith, *Phys. Rev. B* **2006**, *73*, 235104.
[51] N. Baier, A. Brambilla, G. Feuillet, S. Renet, *Nucl. Instrum. Methods Phys. Res., Sect. A* **2006**, *563*, 155.
[52] Y. Cui, P. Bhattacharya, A. Burger, D. Johnstone, *J. Phys. D: Appl. Phys.* **2013**, *46*, 305103.
[53] M. Tapiero, N. Benjelloun, J. P. Zielinger, S. El Hamd, C. Noguet, *J. Appl. Phys.* **1988**, *64*, 4006.
[54] O. Yoshie, M. Kamihara, *Jpn. J. Appl. Phys.* **1983**, *22*, 629.
[55] If the trap density, capture cross section, and thermal velocity are 10^{16} cm^{-3}, 10^{-11} cm^2, and 10^7 cm s^{-1}, respectively, then we would have a Shockley–Read–Hall lifetime of 1 ps. This is much smaller than the lifetime we measured in Figure 2d, and it may be that we are overestimating the capture cross section in the PICTS measurements by assuming it to not change with temperature. Nevertheless, if we assume the capture cross section and thermal velocity to remain the same, increasing the trap density by four orders of magnitude would decrease the lifetime by four orders of magnitude, well below the lifetimes present in BiOI.
[56] X. Ren, J. Yao, L. Cai, J. Li, X. Cao, Y. Zhang, B. Wang, Y. Wei, *New J. Chem.* **2019**, *43*, 1523.
[57] W. Zeng, J. Li, L. Feng, H. Pan, X. Zhang, H. Sun, Z. Liu, *Adv. Funct. Mater.* **2019**, *29*, 1900129.
[58] R. L. Z. Hoye, L. Eyre, F. Wei, F. Brivio, A. Sadhanala, S. Sun, W. Li, K. H. L. Zhang, J. L. MacManus-Driscoll, P. D. Bristowe, R. H. Friend, A. K. Cheetham, F. Deschler, *Adv. Mater. Interfaces* **2018**, *5*, 1800464.
[59] J. C. Balland, J. P. Zielinger, M. Tapiero, J. G. Gross, C. Noguet, *J. Phys. D: Appl. Phys.* **1986**, *19*, 71.
[60] D. Bozyigit, M. Jakob, O. Yarema, V. Wood, *ACS Appl. Mater. Interfaces* **2013**, *5*, 2915.